Lightweight Metal Stamping Optimization Enabled by Artificial Intelligence

Participants from ORNL: William Halsey, Seokpum Kim, Rich Davies, Vincent Paquit

Participants from USCAR: Krishna Murali, Sathya Dev, Liang Huang, Kaiping Li, Andrey Ilinich, Weidong Wu, Lu Huang, Thomas Stoughton

Participant from AutoForm: Kidambi Kannan

Date: March 2025

Final Technical Report
ORNL/SPR-2024/3746

CRADA Number
NFE-21-08589

DOCUMENT AVAILABILITY

Reports produced after January 1, 1996, are generally available free via US Department of Energy (DOE) SciTech Connect.

Website http://www.osti.gov/scitech/

Reports produced before January 1, 1996, may be purchased by members of the public from the following source:

National Technical Information Service
5285 Port Royal Road
Springfield, VA 22161
Telephone 703-605-6000 (1-800-553-6847)
TDD 703-487-4639
Fax 703-605-6900
E-mail info@ntis.gov
Website http://www.ntis.gov/help/ordermethods.aspx

Reports are available to DOE employees, DOE contractors, Energy Technology Data Exchange representatives, and International Nuclear Information System representatives from the following source:

Office of Scientific and Technical Information
PO Box 62
Oak Ridge, TN 37831
Telephone 865-576-8401
Fax 865-576-5728
E-mail reports@osti.gov

The information, data, or work presented herein was funded in part by the Vehicle Technologies Office, the Office of Energy Efficiency and Renewable Energy (EERE), U.S. Department of Energy, under Award DE- EE0006926

Lightweight Metal Stamping Optimization Enabled by Artificial Intelligence

Principal Investigator: Seokpum "Pum" Kim
Organization: Oak Ridge National Laboratory
Address: P.O. Box 2008. Oak Ridge, TN 37831
Phone: 865-574-6357
Email: kimsp@ornl.gov

Participants (ORNL): William Halsey, Seokpum Kim, Rich Davies, Vincent Paquit

Participants (USCAR): Krishna Murali, Sathya Dev, Liang Huang, Kaiping Li, Andrey Ilinich, Weidong Wu, Lu Huang, Thomas Stoughton

Participant (AutoForm): Kidambi Kannan

Date Published: 3/2025

Manufacturing Demonstration Facility (MDF)
Manufacturing Science Division, Oak Ridge National Laboratory (ORNL)
Knoxville, TN 37932
US. DEPARTMENT OF ENERGY
Under contract DE-EE0006926

Project Period
(01/2022 – 09/2024)

Approved For Public Release

TABLE OF CONTENTS

List of Acronyms

USCAR – US Council for Automotive Research. The members of USCAR are Ford, GM, and Stellantis.
AI – Artificial Intelligence
NN – Neural Network, full form: Artificial Neural Network
FCNN – Fully Connected Neural Network
MFA – Max Failure Advanced
MLP – Multi-Layer Perceptron
MSE – Mean Square Error
MAPE – Mean Absolute Percent Error
ADAM – Adaptive moment estimation
ReLU – Rectified Linear Unit
GUI – Graphical User Interface

1. EXECUTIVE SUMMARY

Successfully manufacturing an automotive body structure made via the sheet metal stamping process depends upon simultaneous consideration of component design, tooling design, stamping process control, and material properties. In many cases, introducing lightweight sheet materials (e.g., aluminum alloys, magnesium alloys, advanced high strength steels) holds the potential to significantly reduce vehicle weight, but challenges the stamping process by introducing materials with inherently less ductility. Successful and repeatable applications require co-developing the stamping process controls with the varying material properties, including formability. During the stamping process, as soon as the forming limit of the sheet is exceeded, the material shows localized necking which quickly leads to splits. Controlling process variability to avoid these material splits will enable deployment of less formable, lighter, and stronger materials for stamped automotive components.

A typical optimization procedure for manufacturing requires an iterative process involving parameter setting, execution of computational simulations, and modifying the parameters. The entire process demands substantial computational time, making it impractical for real-time feedback towards rapid corrective actions required for in-line control for running production processes. To overcome this challenge, artificial intelligence (AI) can be leveraged to determine optimal manufacturing parameters within a single manufacturing cycle time. This research proposes an in-line optimization framework incorporating a trained AI model to predict kidney-shaped die forming. Preliminary results indicate that the AI framework can accurately predict draw-in values based on a given parameter set, a process referred to as forward prediction. Furthermore, the AI framework can also predict the optimal parameter set that leads to the desired draw-in values, referred to as inverse optimization (or backward prediction).

This research has been performed in collaborations with USCAR (US Council for Automotive Research) and AutoForm. The members of USCAR are Ford, GM, and Stellantis.

2. INTRODUCTION

Sheet metal stamping is a critical manufacturing technique in the automotive industry, particularly for producing body structure components. The quality of the manufactured parts highly depends on complex interplay of factors, including sheet material properties, lubrication conditions, die geometry, surface wear, and press operations dynamics. Some of the common issues in stamping process include inconsistencies in dimensions, forming severity, and surface quality of stamped parts. Figure 1 shows some of the issues predicted through computational simulation, including potential split, wrinkles, skid marks, edge cracks, and springback.

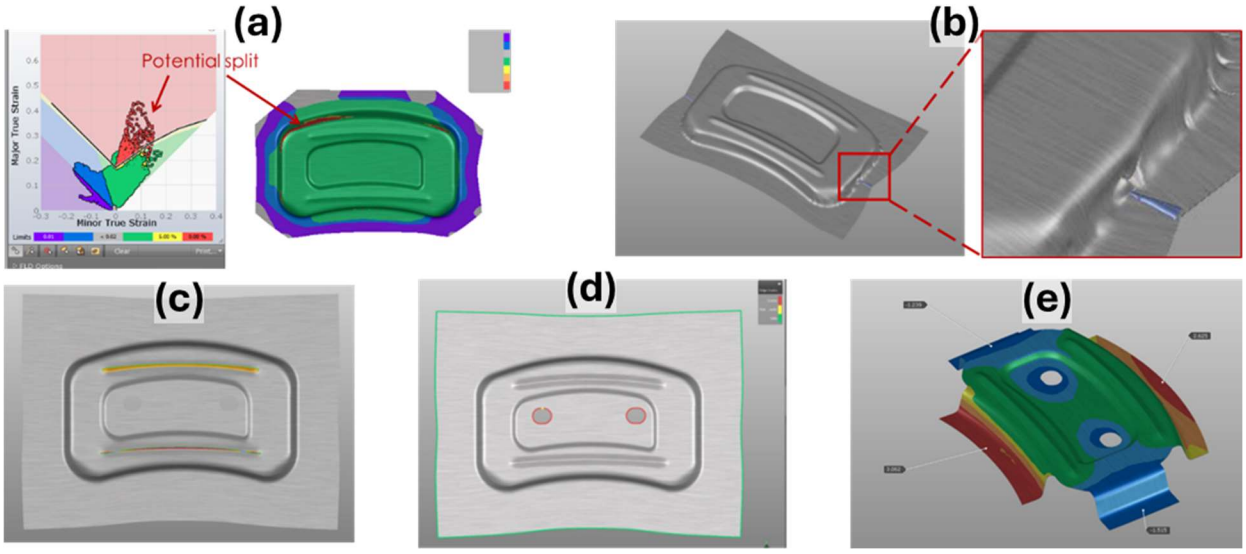

Figure 1 – Common issues in stamping predicted through simulation (software: AutoForm). (a) Potential split, (b) wrinkles, (c) skid marks, (d) edge cracks, (e) springback.

The automotive industry's push towards vehicle lightweighting necessitates the use of lightweight materials such as aluminum alloys and advanced high strength steels and calls for the use of precise process control in stamping operations. Therefore, there is a need for advanced control algorithms that can manage process variability and optimize stamping parameters in real-time to prevent material failures and ensure consistent part quality.

Traditional optimization procedures for sheet metal stamping process typically involve iterative cycles of parameter setting, computational simulations, and subsequent modifications, which is often time-consuming and impractical for providing real-time feedback in a production environment. The top flowchart in Figure 2 illustrates this process. Artificial intelligence (AI) and machine learning (ML) techniques can offer promising solutions for rapid, in-line process optimization, which may be implemented to address the limitations of the traditional procedure.

In this project, we propose an innovative approach to developing an AI-driven stamping process optimization. To expedite the development, the research initially focuses on a simplified product geometry, referred to as a kidney die panel. Various forming quality issues can be realized during the kidney die forming by changing materials or process parameters, making this design a representative candidate for the development of core ML algorithms without the additional complexities introduced by more intricate automotive geometries. After the development, the AI-driven optimization framework is applied to a door frame.

The proposed framework incorporates a trained AI model capable of both forward prediction and inverse optimization, as illustrated in the middle and bottom flowcharts in Figure 2. Forward prediction involves accurately estimating the stamped part quality through draw-in values based on given parameter sets. The inverse optimization determines the optimal parameter set to achieve

desired draw-in values. This dual-capability system aims to provide rapid, in-line optimization within a single manufacturing cycle time, representing a significant advancement in stamping process control.

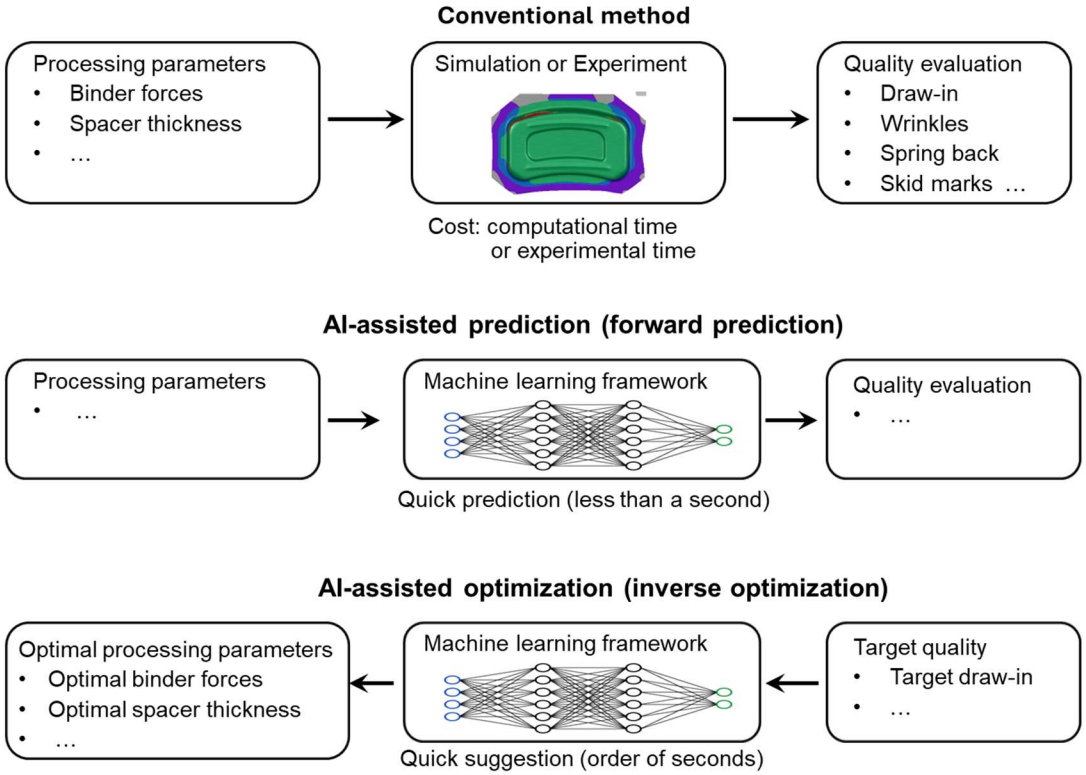

Figure 2: Flowcharts of (a) a conventional method for stamping optimization, (b) AI-assisted prediction (forward prediction), and (c) AI-assisted optimization (inverse optimization)

This research establishes a foundation for AI-driven process control in sheet metal stamping. The successful implementation of the system shows the potential to significantly improve part quality consistency, reduce material waste, reduce production down time and delays, and it will facilitate the broader adoption of lightweight materials in automotive manufacturing.

3. STAMPING SIMULATION

The generation of comprehensive training data is crucial for an effective AI-drive stamping optimization model. Although an AI-driven stamping optimization model can significantly reduce computation time compared to traditional simulation methods, this speed increase comes at the cost of extensive initial data preparation. The model requires a large, well-labeled dataset for training. To generate this dataset efficiently, we utilized AutoForm [1], a commercial finite element analysis (FEA) tool for stamping simulations. The FEA tool allowed us to simulate a wide range of stamping scenarios and parameter combinations, providing the diverse data needed to train a robust AI model. This simulation-based approach enabled us to create a comprehensive synthetic dataset, while still capturing the complex physics of the stamping process.

3.1 Geometry and Simulation Setup

For initial development and validation, a kidney die geometry was selected as the test case as shown in Figure 3. This geometry was chosen for its versatility in capturing various deformation modes while maintaining relatively simple shape compared to automotive components in production. The nominal process parameters were chosen to produce a feasible part with acceptable forming quality, providing a baseline for comparison.

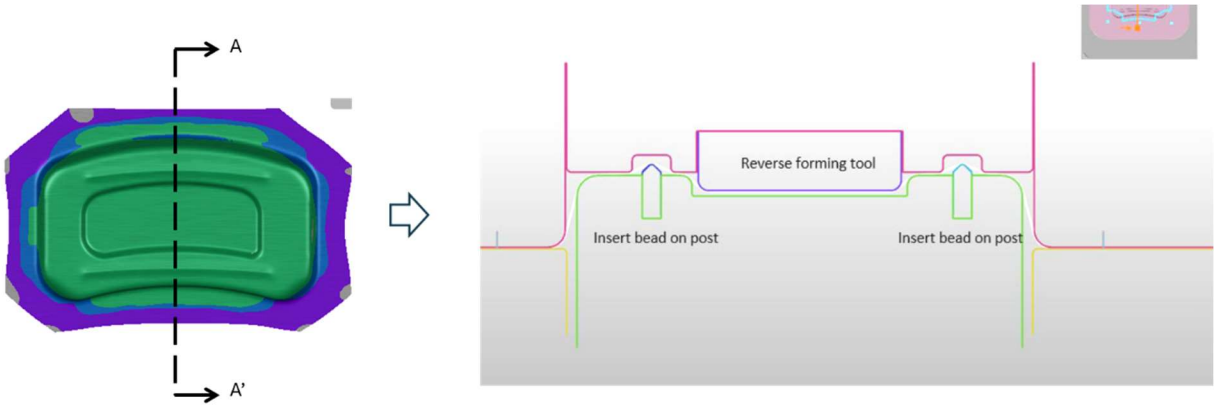

Figure 3. Kidney die geometry for stamping optimization (Left) top view, (Right) cross-section shape.

The simulation parameters included both controllable and uncontrollable parameters. Controllable parameters are: individual draw bead forces, bead spacer thickness, total binder force, and friction coefficient. Figure 4 shows the stamping parameters defined in AutoForm. The simulation setup incorporated systematic variation of these parameters within predefined ranges, allowing for the coverage of different potential manufacturing scenarios. AutoForm Sigma was configured to generate 880 distinct simulation cases, providing sufficient data for AI model training.

Controllable Variables

Name	Dependenc	From	To
All Operations			
frictionCoefficient		0.08	0.2
Mat01_rm		0.458	0.688
Mat01_Sigma0		95 MPa	163.8 ...
Mat01_Tensile	Positive	212 MPa	253 MPa
D-20			
CntrLeft		0.3	0.9
CntrLwr		0.3	0.9
CntrRight		0.05	0.5
CntrUpr		0.4	0.9
constantForce		100 kN	300 kN
LwrLeft		0.05	0.5
LwrRight		0.05	0.45
thickness_2		0 mm	0.2 mm
UprLeft		0.05	0.5
UprRight		0.15	0.6

Delete | Edit | Go To

Uncontrollable Variables

Name	Min	Max
All Operations		
thickness	0.85 mm	0.95 mm

Figure 4 – Ranges for input parameters for AutoForm's sigma trials that were used to create the

training dataset.

3.2 Simulation Results

The AutoForm sigma trials feature was used to generate a dataset using randomly chosen material properties and process parameters as dictated by the respective ranges. Subsequently, the simulation was run, and quality metrics were recorded for geometrically relevant locations of the stamped component. A total of 880 processing scenarios were generated and simulated as sigma trials to form the basis of the dataset for the kidney die geometry. This dataset was used to train a neural network surrogate model. Appendix 1 – Simulation quality metrics and locations – shows the quality metrics and locations where data were generated via the simulation. Table 1 enumerates the localized quality metrics that were simulated and recorded.

Table 1 – Description of key performance indicators that were simulated.

Feature name	***Description***
Draw-In	• Material inflow at a specific location during stamping • Eight locations around the blank edge were monitored for material inflow
Max Failure Advanced (MFA) Criterion	• Value that is correlated with the potential for material splitting • Multiple critical zones were established to monitor potential splitting • Measurements compared major strains against the material's forming limit curve
Potential Wrinkling	• Indicator of amount and severity of wrinkling • Areas prone to compression and wrinkling were identified based on engineering experience • Metrics were collected to quantify the severity of potential wrinkling
Thinning	• Material thinning as a percent change from original blank thickness
Springback	• Material displacement in the normal direction after stamping

Each of the quality predictors are real values. Based on the design requirements for the component, the real values can also be explicitly mapped into classes that represent a flaw or not for the given flaw type and location of interest.

3.3 Data Preparation for AI Training

After the data set was generated, several pre-processing steps were performed before training the neural network. Each of the features are scaled between 0 and 1 using min-max scaling [2]. Also, as discussed previously, each of the target features are real values that can be explicitly mapped to a class that represents a flaw or not. This mapping and the corresponding classifications

are necessary when leveraging the surrogate model for optimization. Several distinct functions may be employed to perform this class membership function mapping as shown in Figure 5. Initially, the simplest class membership function, option 1, a simple threshold, was used.

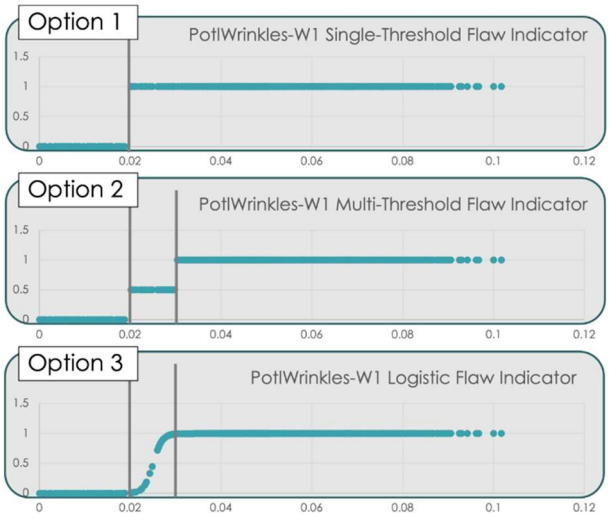

Figure 5 – Several possible class membership functions to transform real values from simulation to a flaw classification.

This mapping may be done at two distinct moments in the workflow. First, the mapping may be done a priori where the dataset is augmented with class membership for each output feature respectively. In this form, the model learns the regression and classification simultaneously and independently. Initially, for more advanced optimization objectives, these class membership features were precalculated and added to the dataset before training the neural network. This approach will be further outlined in Section 5, specifically Section 5.2 Optimizing to Remove Splitting Directly.

4. ARTIFICIAL INTELLIGENCE FRAMEWORK

For this work, a neural network is trained to serve as a surrogate model. The model is trained to predict performance metrics at locations of interest across the geometry given a set of material properties and processing parameters. The trained network may then be used to perform parameter optimization to reduce the occurrence of flaws given a suboptimal combination of material properties and processing parameters. The Python library Keras [3] was used for creating and training the neural network and for creating custom network layers for optimization.

4.1 Numerical Modeling (Framework)

The target application of in-line process optimization and the inherently tabular nature of the

data led to the choice of a Multi-Layer Perceptron (MLP) neural network for the surrogate model. The default MLP network consists of an input layer, three hidden layers with 100 neurons each, and the output layer as shown in Figure 6.

.

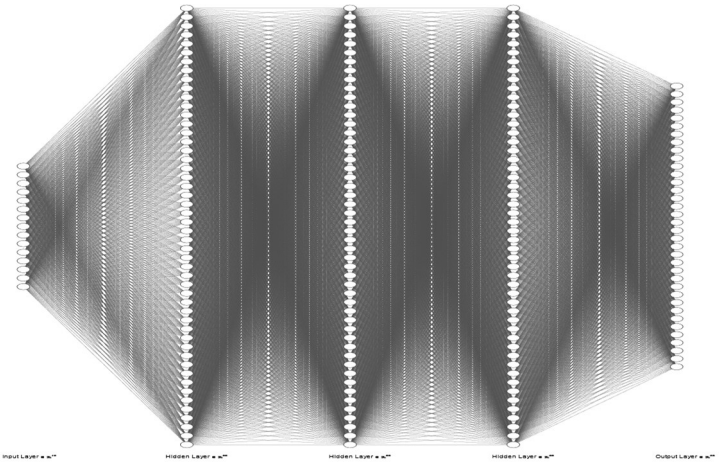

Figure 6 – Default model architecture with three hidden layers with 100 hidden neurons each.

4.2 Hyperparameter Settings

The model hyperparameters used while developing the framework were largely unchanged. The values are shown in Table 2. Future work will include hyperparameter optimization.

Table 2 – Model hyperparameters

Hyperparameter	Value
Train/Test Split	80%/20%
Data Normalization	Min-Max Scaling
Loss	MSE
Optimizer	ADAM
Epochs	250
Learning Rate	0.001
Epsilon	1.e-5
Hidden layer activation	'ReLU'
Output layer activation	'sigmoid'

4.3 Training and Convergency (Loss) with Epoch

Initially, draw-in was used to evaluate the surrogate model's performance. The reported error

is the Mean Absolute Percent Error (MAPE). Analysis of the results showed differing levels of accuracy depending on whether a physical split had occurred or not. Table 3 below shows the average MAPE for the test data, and Appendix 2 – Surrogate model training results – shows comparisons of predicted and simulated draw-in for several representative test cases.

Table 3 – Surrogate model performance for predicting draw-in.

Description	***MAPE***
Cases with splitting	11.1%
Cases with no splitting	4.7%
Full test set	6.4%

In addition to the material draw-in, the surrogate model was also simultaneously trained to predict the other quality metrics, such as MFA criterion and potential wrinkling, at their respective locations. Training the model to predict all of the targets simultaneously helps the model generalize and not overfit the training samples. Additionally, the model can be trained to perform a classification task to predict if a given quality metric at a given location represents a flaw or not. These predictions may be used for more complex optimization objectives.

5. PERFORMANCE OF THE AI FRAMEWORK

Once the surrogate model is trained, it is ready to be used for parameter optimization. Neural networks have several interesting properties that will facilitate optimization. First, neural networks are widely acknowledged to be universal function approximators. Once trained, they represent complex non-linear function. Additionally, they also represent differentiable functions; this is why they are trainable using gradient-based methods.

So, once a model is trained, the same mechanics that were used to train the network may also be used for parameter optimization. However, the weights of the network that were learned during initial training are frozen and remain unchanged during optimization. The process is outlined in the flow chart in Figure 7.

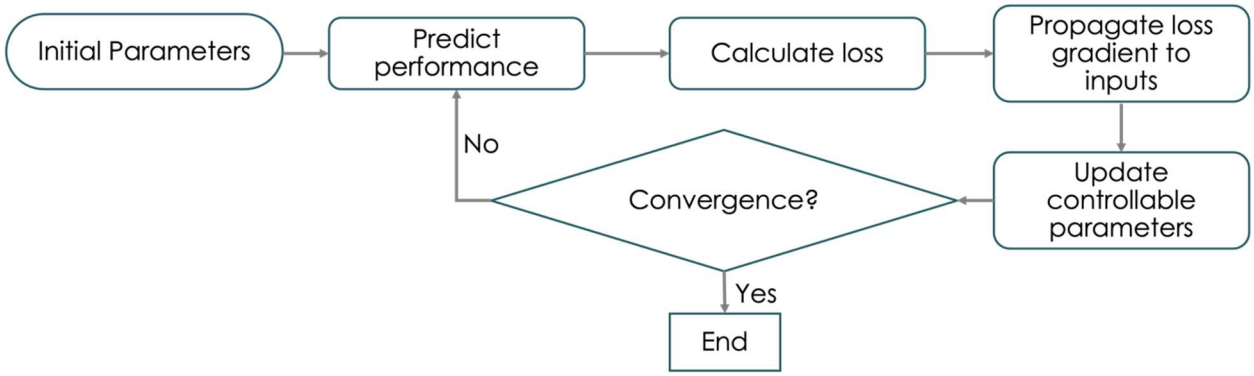

Figure 7 – Algorithm for process parameter optimization.

5.1 Nominal Draw-In as Optimization Objective

We used this approach to optimize the processing parameters from the test cases. Appendix 3 – Optimization for draw-in" shows the evolution of the processing parameters and targets as well as simulations of three representative cases from the test set. After optimization the MAPE for draw-in from the test cases compared to the nominal draw-in was 1.8 percent.

The draw-in values of the optimized parameter sets closely approximated the nominal draw-in. However, further analysis showed that potential splitting, indicated by an MFA criterion value greater than one, still occurred for some optimized parameter sets. Generally, initial parameter sets that resulted in significant splitting initially were likely to have unacceptable MFA criterion values even after optimization. Figure 8 shows a representative case where the optimized parameters remove even potential splitting; Figure 9 shows a representative case where potential splitting persists even after optimizing to match nominal draw-in, though maximum strains were significantly reduced.

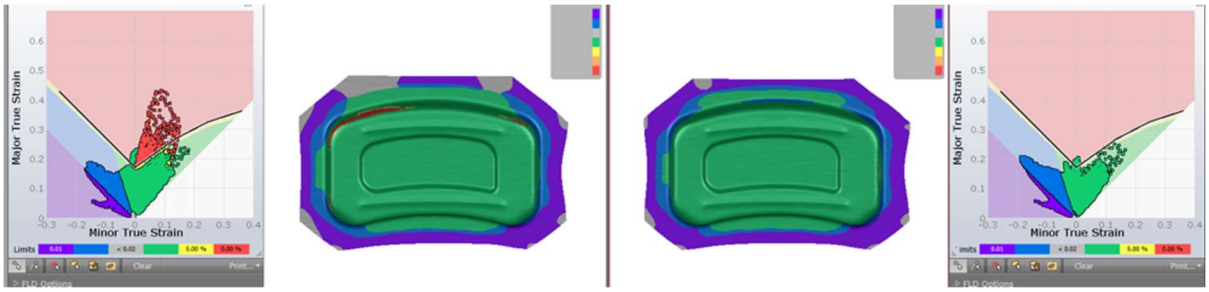

Figure 8 – a representative case where no physical splitting occurs with the original processing parameters and optimized parameters remove even potential splitting.

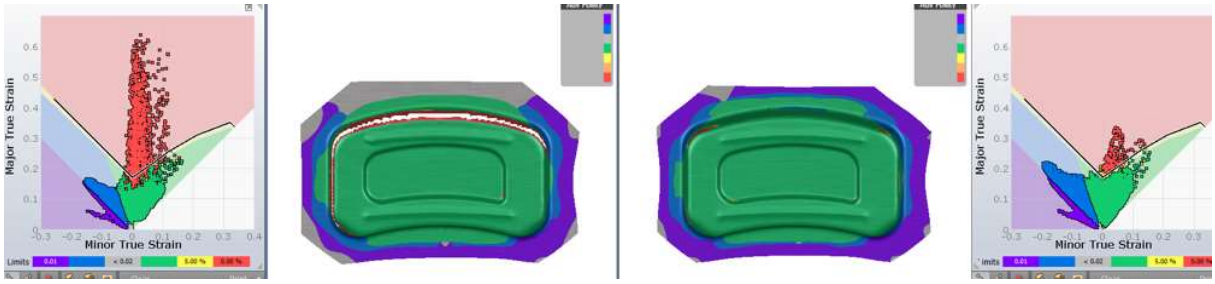

Figure 9 – A representative case where physical splitting does occur with the original processing parameters, and potential splitting persists even after optimizing to match nominal draw-in.

So, while draw-in is a reasonable proxy for part quality, using it as the sole target for stamping process optimization may not yield acceptable results. As such, we also tried other more complex optimization objectives.

5.2 Optimizing to Remove Splitting Directly

Our next goal was to account for splitting directly during optimization. This was accomplished by augmenting the dataset with class membership, or flaw indicator, features. Initially, we used a threshold of 0.9 for the MFA criterion. Figure 10 shows the mapping of MFA to flaw classification for location *'Z5'* for the training data set. Specifically, a value of '0' correlates to MFA values lower than 0.9; and a value of '1' correlates to MFA values higher than 0.9.

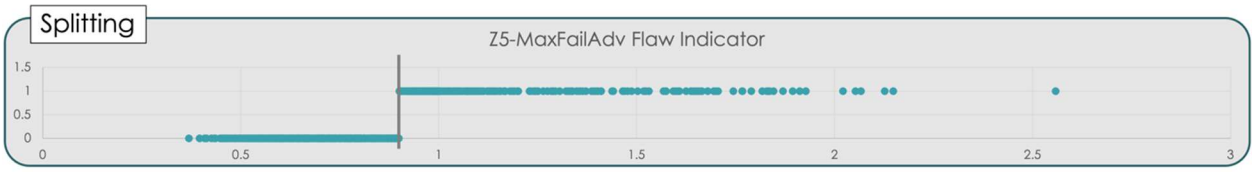

Figure 10 – Flaw indicator feature mapping for MFA at location five.

Once trained to predict these additional features, they may be used during parameter optimization. During optimization the target for these features if '0' representing no potential splitting at any location. This contrasts with an optimization objective where specific MFA values would have to be chosen arbitrarily for each location.

Using this method, two optimization objective functions were tested that would account for splitting directly on the processing parameter sets suggested by OEM formability engineers. The first was simultaneously attempt to match nominal draw-in while removing splitting. The second optimization objective was perhaps more intuitive: have two rounds of optimizations and attempt to match nominal draw-in the first and then remove any remaining splits in the second. Simulations of optimized parameters for four representative cases for both optimization objectives are shown in Figure 11 and Figure 12, showing persistent potential of splits in both cases after optimizations, regardless of the objective functions used.

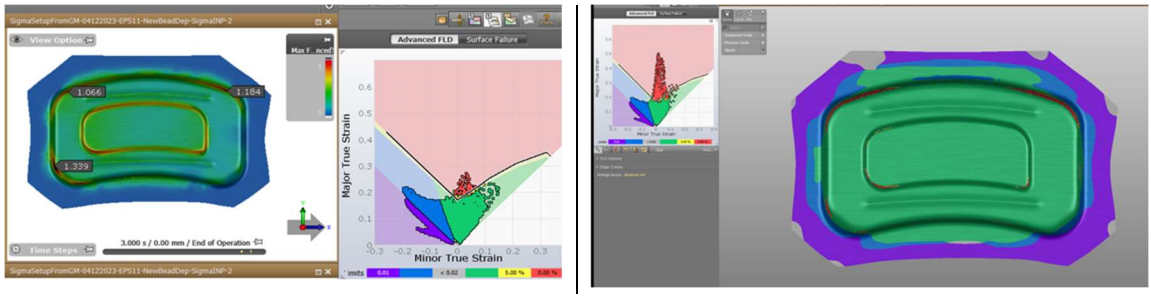

Figure 11 – Optimization objective to simultaneously match nominal draw-in and remove splitting for two new processing parameter test sets from left) GM and right) Ford.

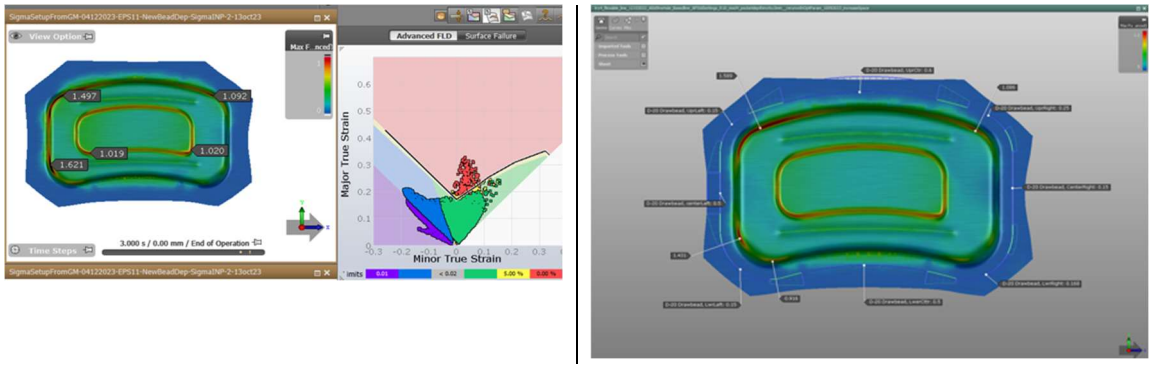

Figure 12 – Optimization objective to serially match nominal draw-in then remove splitting for the test sets from left) GM and right) Ford.

5.3 Removing Process Parameter Constraints

Given the unsuccessful attempts at removing potential splitting, the OEM formability engineers attempted to manually tune the processing parameters to remove splitting, and were able to find processing parameters that yielded successful solutions, shown in Figure 13 and Figure 14. However, those solutions included processing parameters outside of the original ranges specified for data set generation. During optimization processing parameters had been constrained to stay within the original data ranges to ensure that the model would not be extrapolating.

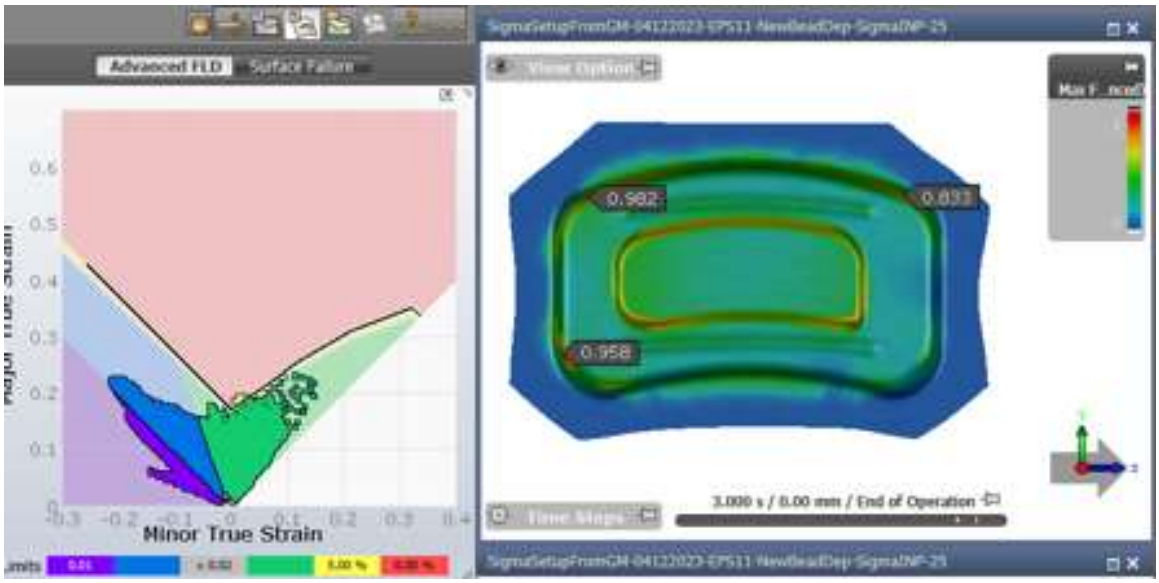

Figure 13 – Manually optimized solution from GM.

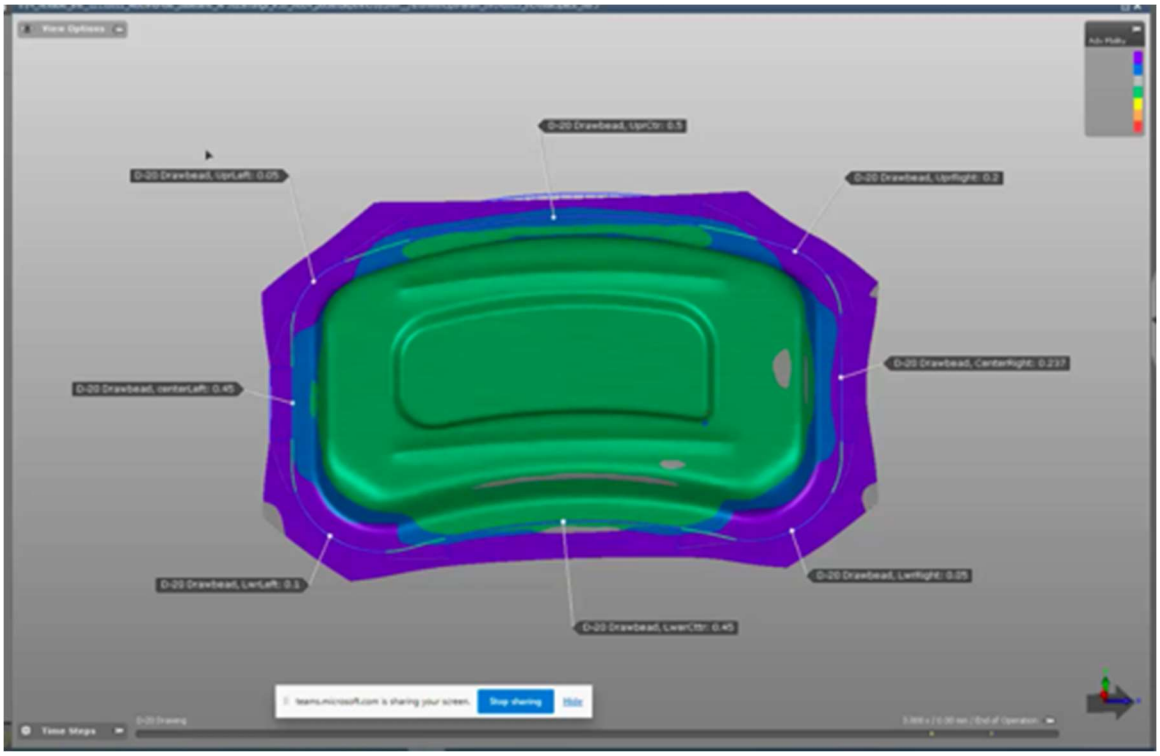

Figure 14 – Manually optimized solution from Ford.

To determine if the model would also be able to find a viable solution, the constraints on the parameter ranges were dropped and the second optimization objective was run again. This time the model was also able to find a set of parameters that yielded an acceptable solution. The simulations for the two cases with the unconstrained optimization are shown in Figure 15 and Figure 16.

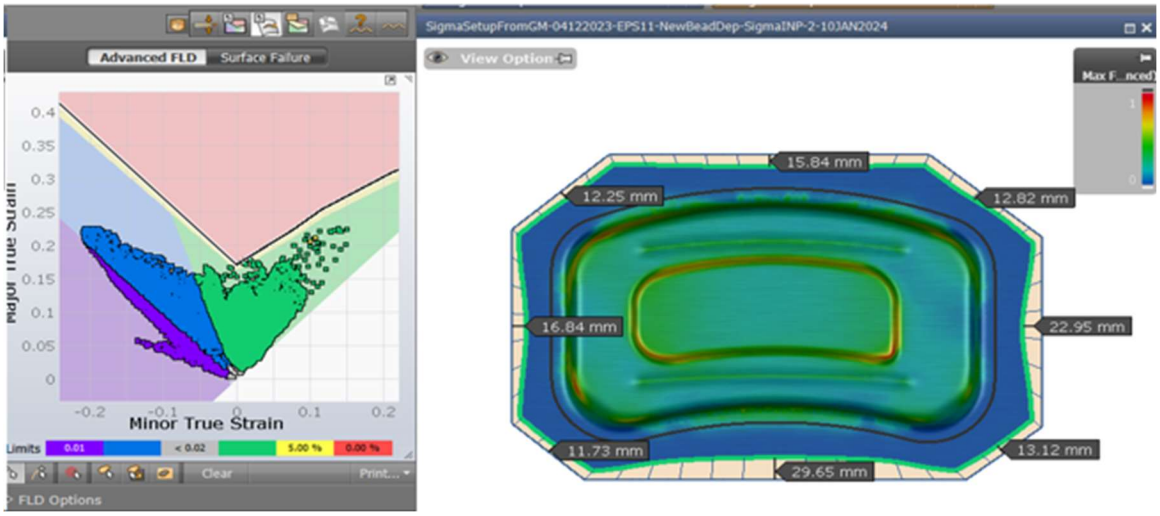

Figure 15 – Optimization objective to serially match nominal draw-in then remove splitting with no constraints on processing parameter bounds for the test set from GM.

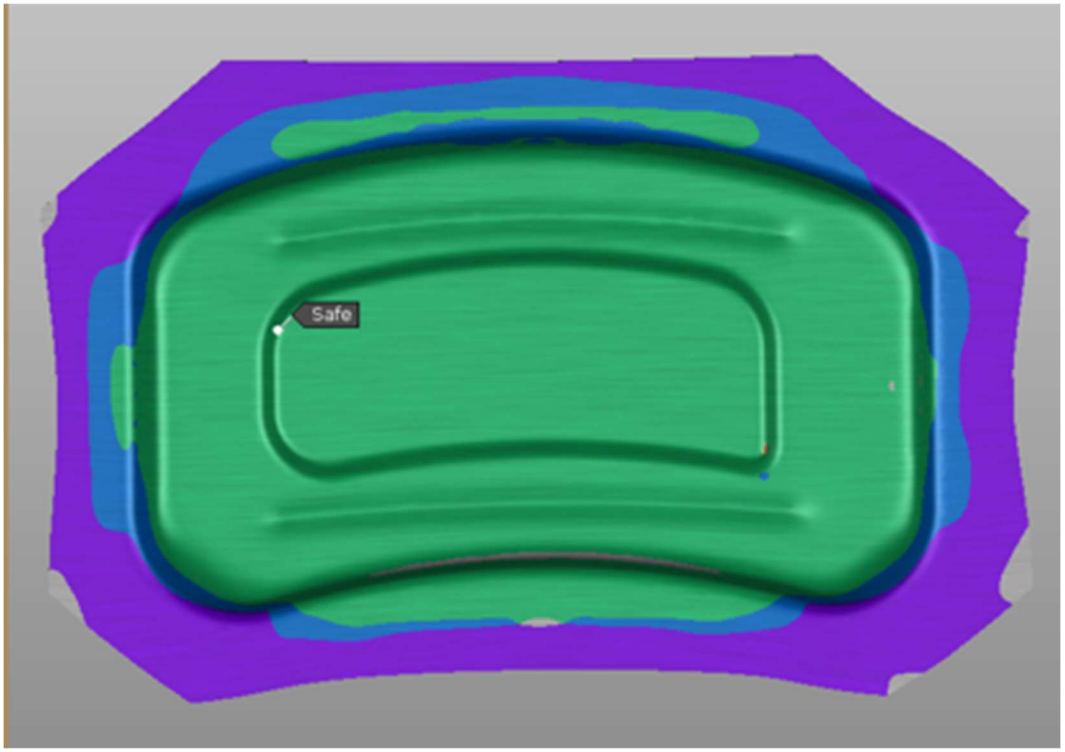

Figure 16 – Optimization objective to serially match nominal draw-in then remove splitting with no constraints on processing parameter bounds for the test set from Ford.

6. APPLICATION TO DOOR PANEL (GEOMETRY IN PRODUCTION)

Upon the success of the trials on the kidney die geometry, the next step was to determine if the framework would be applicable on a geometry currently in production. The framework was applied to a door panel geometry to assess the generalizability of the method to other geometries. The door panel geometry was provided by GM. The geometry has fourteen controllable parameters – twelve secondary draw bead forces, global friction coefficient, and the binder force– that serve as inputs, together with material properties, to simulation and the surrogate model.

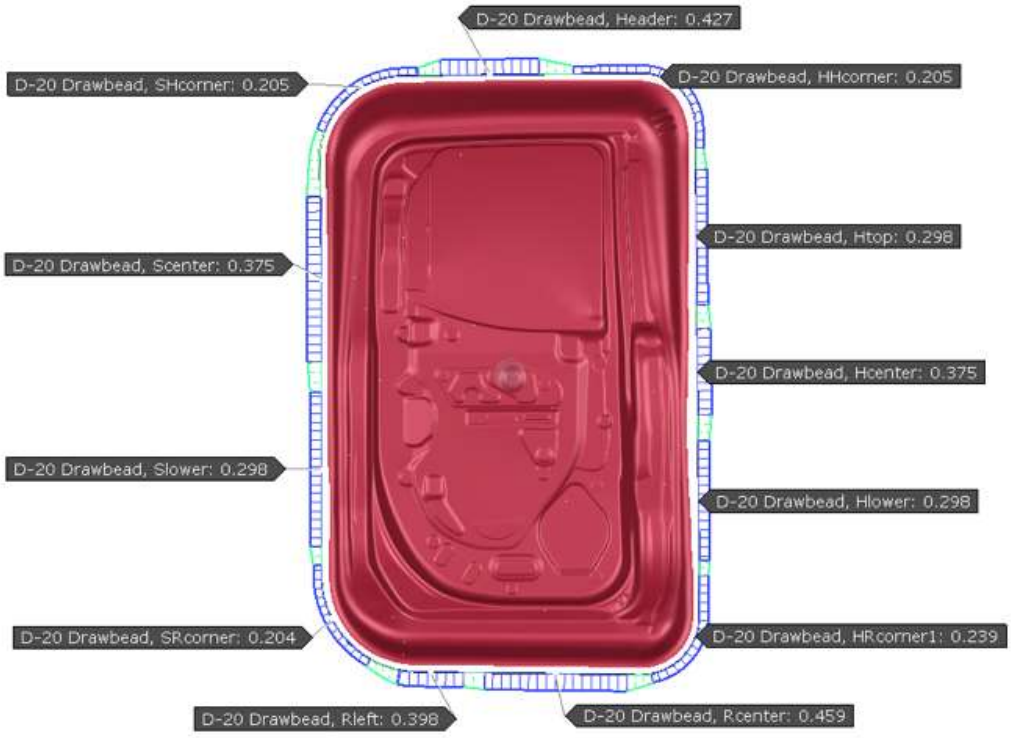

Figure 17 – Door panel geometry and secondary draw beads.

Figure 17 shows the door panel geometry, and one should note that its complexity is significantly greater than the kidney die geometry. The generated dataset consisted of 254 samples. Draw-in was evaluated at nineteen locations, and max failure was calculated at eighteen locations. Optimization was performed in two rounds: round one aimed to match nominal draw-in, and round two's objective was to remove any splitting that remains. The simulation results of initial and final parameter sets are shown in Appendix 3.

7. USER-INTERFACE APP

A GUI program, called st*A*mp*I*ng, was created to facilitate training a surrogate model and leveraging it for optimization. The app offers many configuration options for users to enable them to test and evaluate the framework for different geometries and for different optimization configurations. The packaged program offers configurable inputs and targets for model training and the ability to save and load trained models. Additionally, it allows users to customize optimization rounds and targets. Figure 18 shows a screenshot of the st*A*mp*I*ng program.

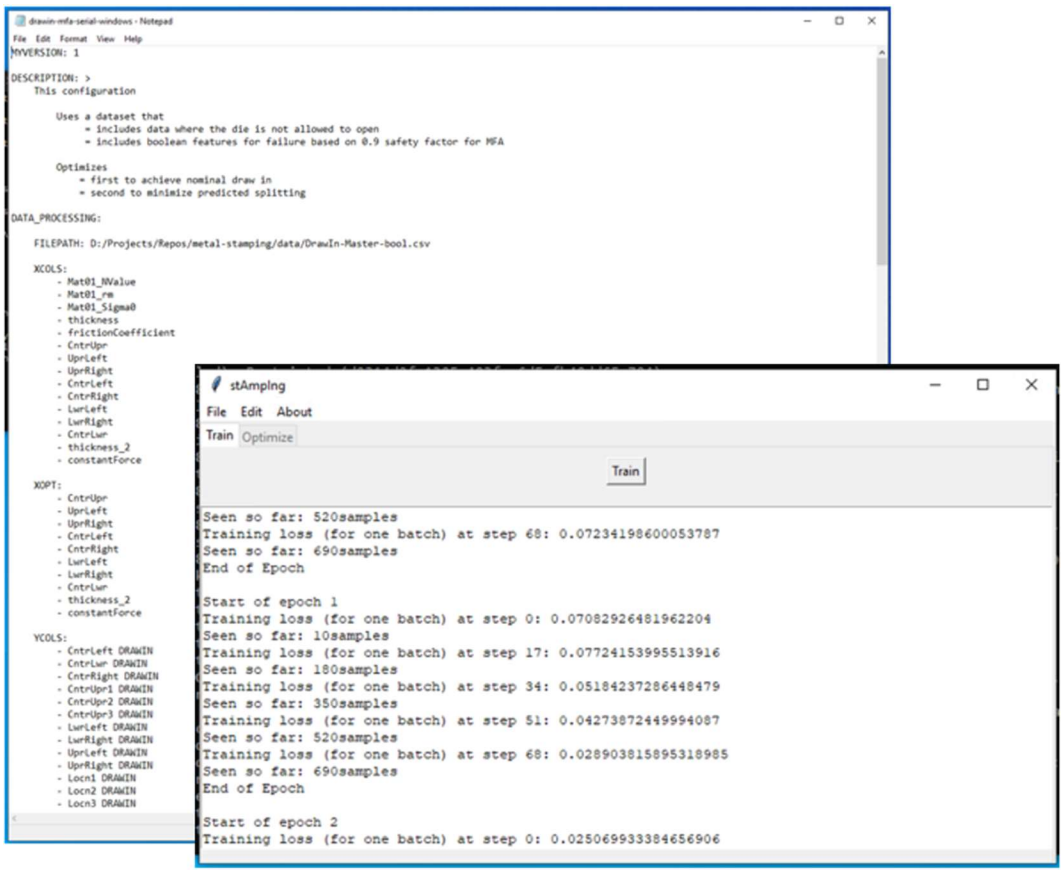

Figure 18 – Screenshot of the program's project specification file and user interface.

8. CONCLUSIONS

In this research, we have successfully developed an innovative AI-driven optimization framework for sheet metal stamping processes and demonstrated its effective performance for automotive applications. The integration of AI with stamping simulation shows a viable path for real-time process optimization. By leveraging AutoForm's finite element analysis to generate training data, we established an accurate AI-based prediction model and a robust AI-based optimization model. The total of 880 simulation cases for the kidney die geometry and the total of 254 simulation cases for the door panel provided sufficient data to train the AI framework capable of predicting multiple quality metrics simultaneously and optimizing the controllable parameters.

The AI-based prediction model showed strong predictive performance, particularly for cases without splitting, achieving an error of only 4.7% (mean absolute percentage error) for draw-in distances. We have also demonstrated that the model can predict multiple quality metrics simultaneously including draw-in, potential splitting, and wrinkling.

The AI-based optimization model was further proven effective in multiple scenarios. In particular, when the model is allowed to suggest optimal stamping parameters without constraints, the stamping parameters suggested by the model led to the most optimal stamping qualities. The

two-step serial optimization approach - first matching nominal draw-in values and then considering potential splitting – produced highly optimal stamping parameters that led to quality stamped parts for both the kidney die and the more complex door panel geometry. The successful scaling from a simplified test case (i.e., kidney die) to a production component demonstrates the high potential of our AI framework for real-world manufacturing applications.

We also developed "st*A*mp*I*ng", a user-friendly interface for the AI software combined with flexible configuration options and the ability to save and load training data for various geometries. This software provides easy accessibility to manufacturing engineers who may not necessarily have expertise in AI or programming.

9. ACKNOWLEDGEMENTS

The authors gratefully acknowledge support from Lightweight Materials Consortium (LightMAT), sponsored by the Vehicle Technologies Office, Office of Energy Efficiency and Renewable Energy, U.S. Department of Energy. The authors also acknowledge support from AutoForm for stamping simulations.

10. Reference

[1] AutoForm, "Sheet metal forming simulation software developer," AutoForm Engineering GmbH, [Online]. Available: https://www.autoform.com/en/.

[2] "MinMaxScaler," [Online]. Available: https://scikit-learn.org/stable/modules/generated/sklearn.preprocessing.MinMaxScaler.html. [Accessed 15 10 2024].

[3] "Keras," [Online]. Available: https://keras.io/. [Accessed 15 10 2024].

Appendix 1 – Simulation quality metrics and locations

Max Failure Adv. – Target is 1.0 (or 0.9 with a 10% safety margin)

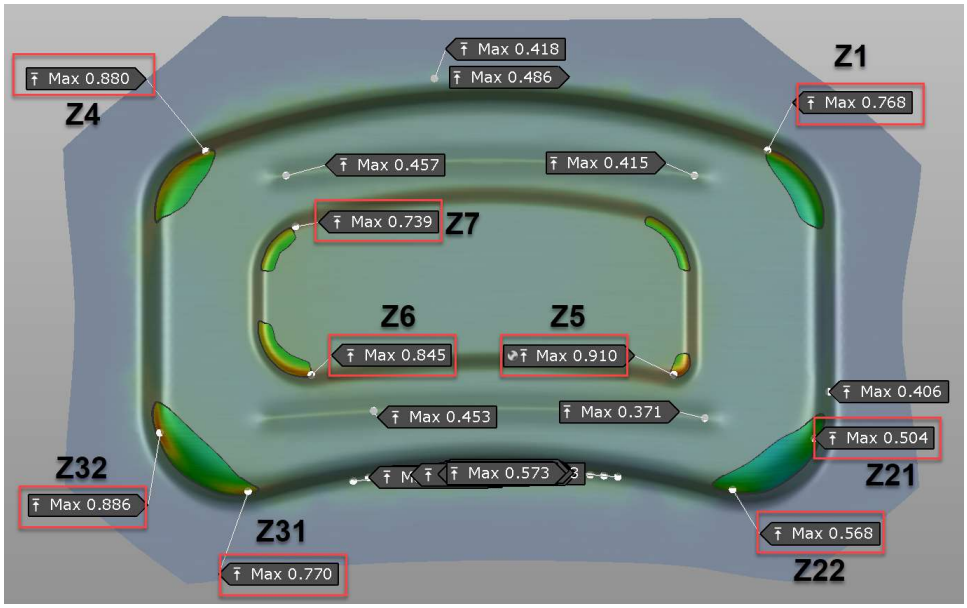

Figure 19 – Locations where max failure advanced criterion, an indicator of possible splits, was evaluated.

Potential Wrinkles – Target is 0.02 (0.03 if 0.02 is not achievable)

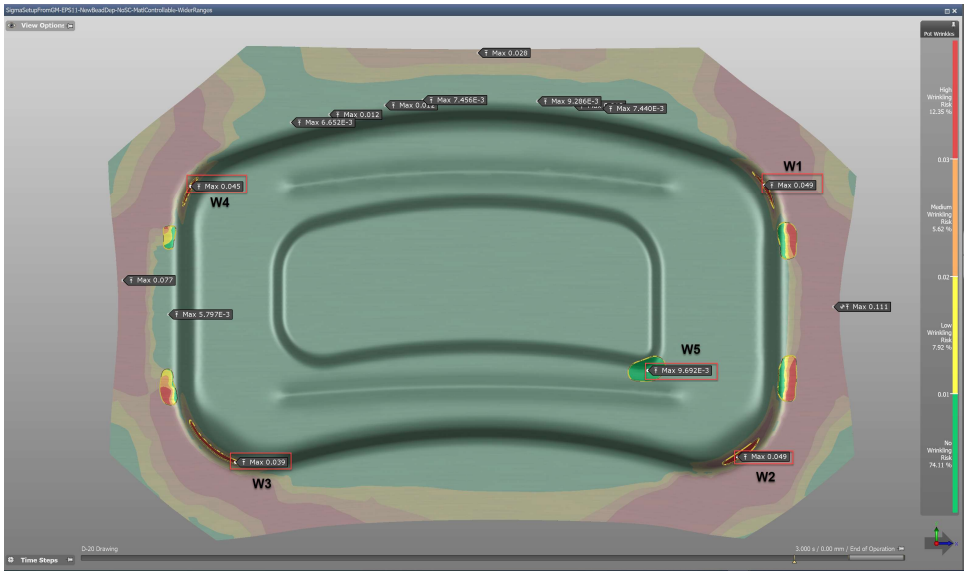

Figure 20 – Locations where potential wrinkling was evaluated.

Product Performance (Required Thinning) – Target is -0.02 (need at least 2% thinning)

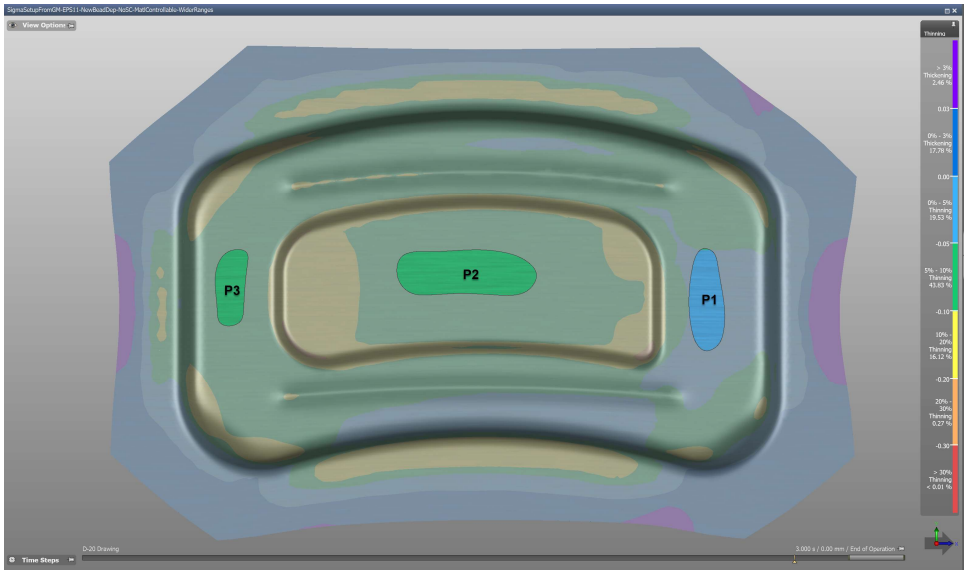

Figure 21 – Locations where material thinning was simulated.

Draw-in – Target is Nominal

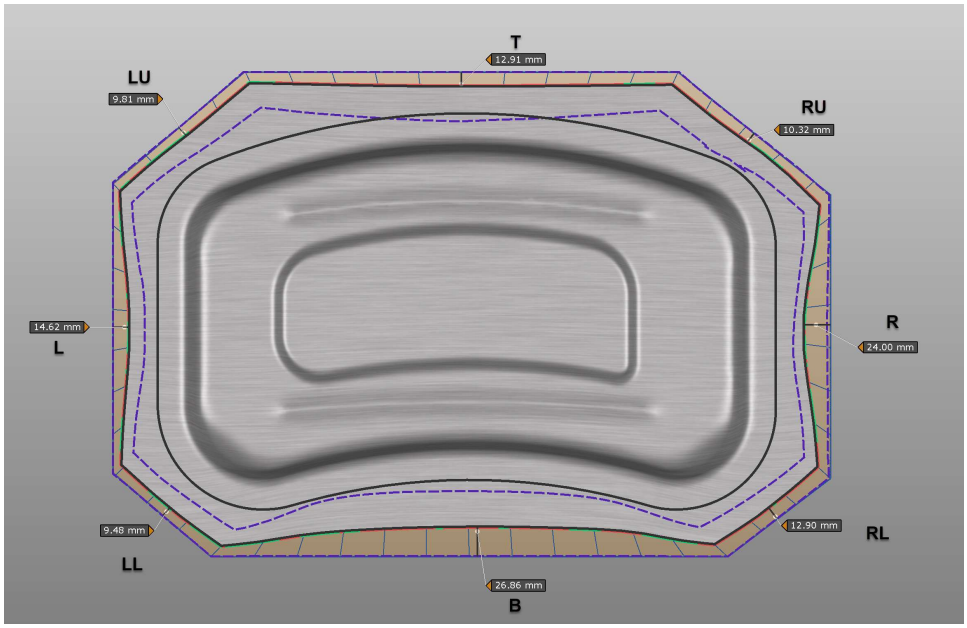

Figure 22 – Locations where draw-in was calculated and the nominal draw-in value for each location.

Springback (Free) was run after T30. Tables were generated at the locations below. Result variable is Material Displacement in the Normal direction. Target is 0mm (since the sheet before springback represents Nominal shape)

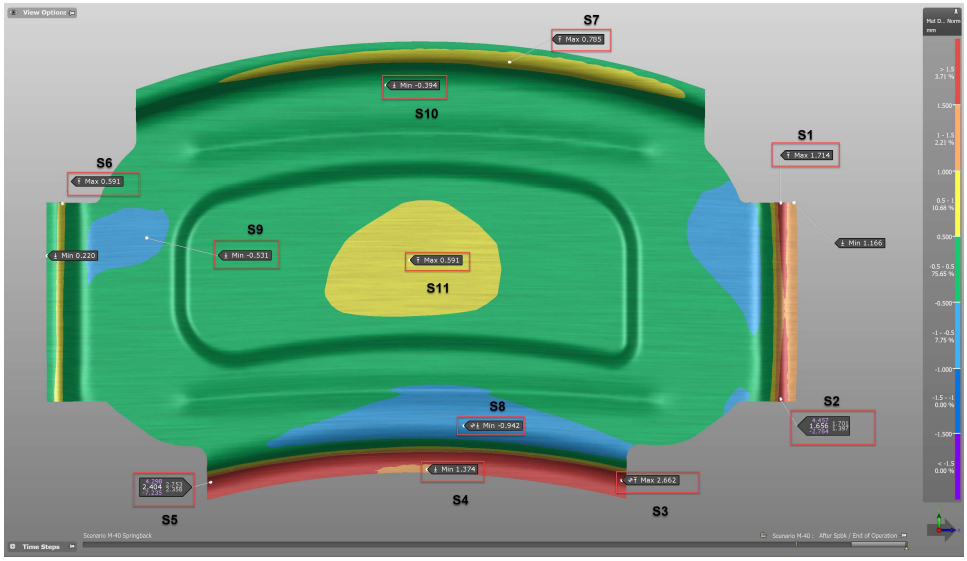

Figure 23 – Locations where material displacement in the normal direction (spring back) was evaluated.

Appendix 2 – Surrogate model training results

Cases with no splits

Sim #1

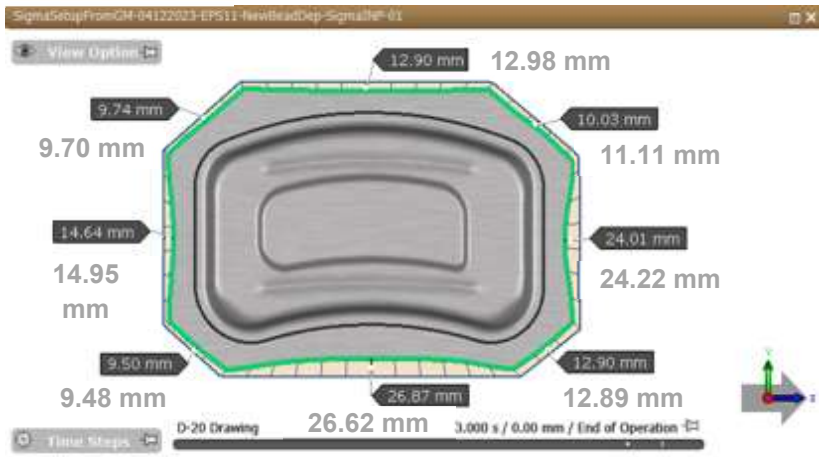

Error: 1.9%

Sim #6

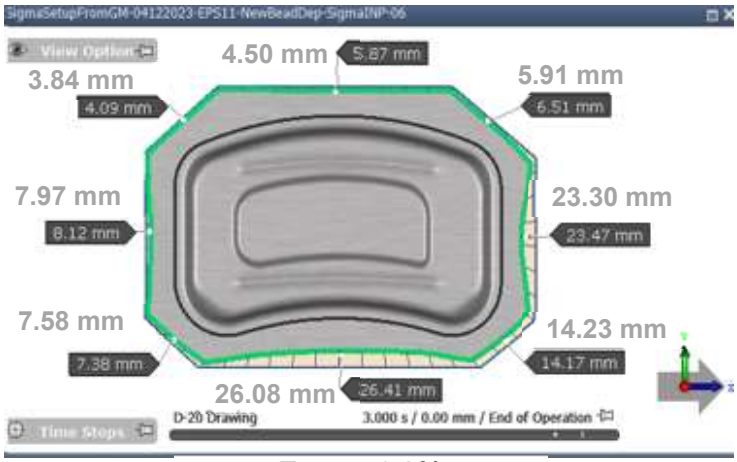

Error : 6.8%

Sim #7

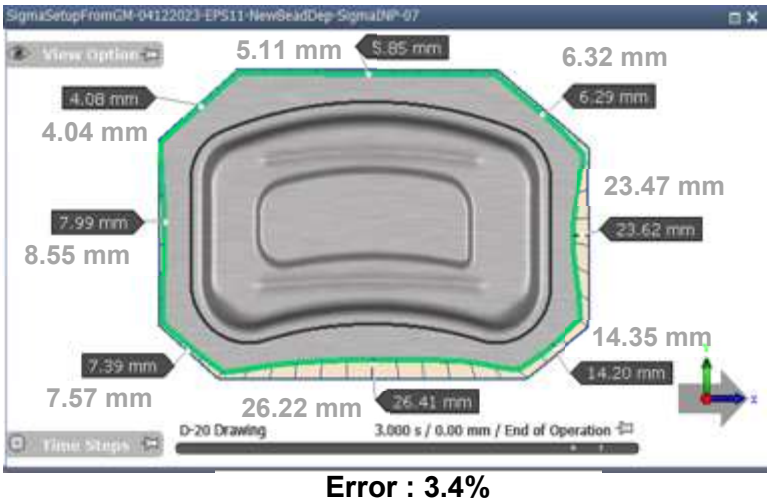

Error : 3.4%

Cases with splits

Sim #2

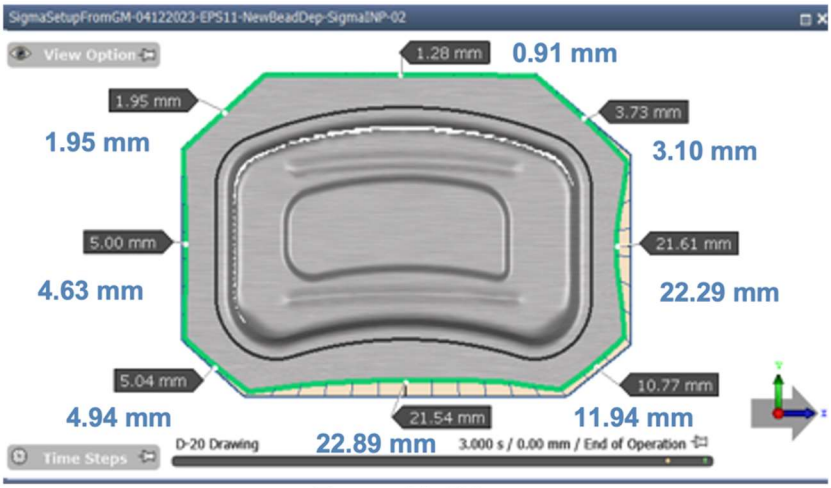

Error: 11.1%

Sim #3

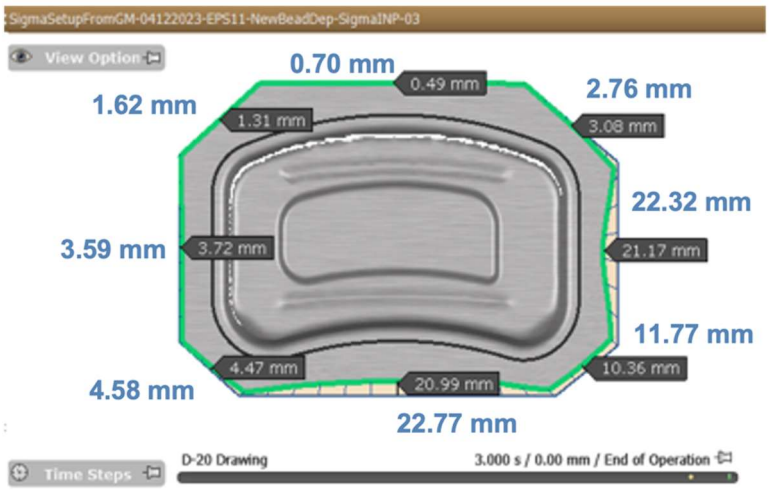

Error: 11.5%

Sim #4

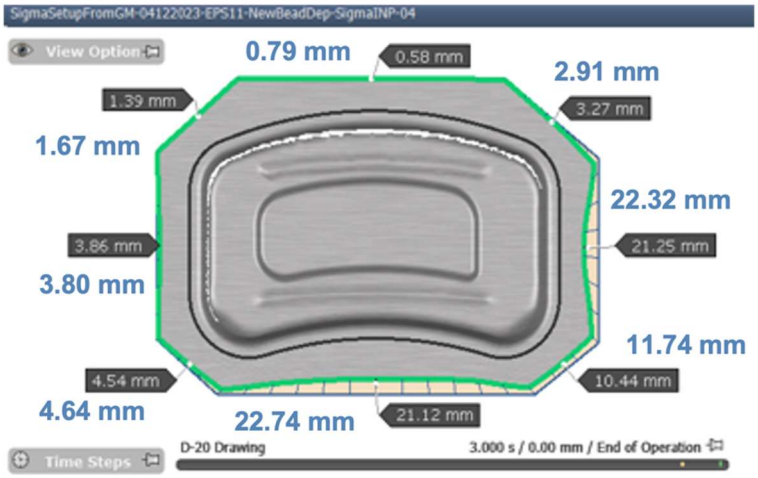

Error: 10.3%

Appendix 3 – Optimization for draw-in

Case 1

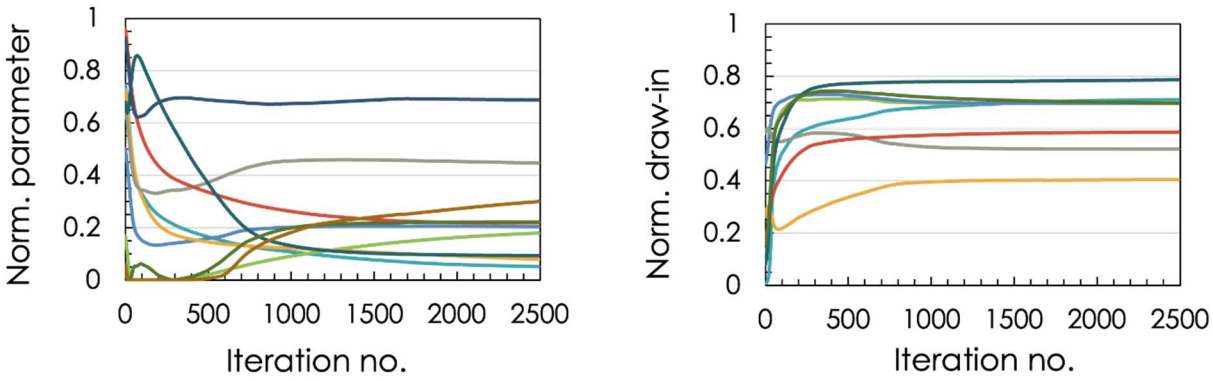

Sim #1

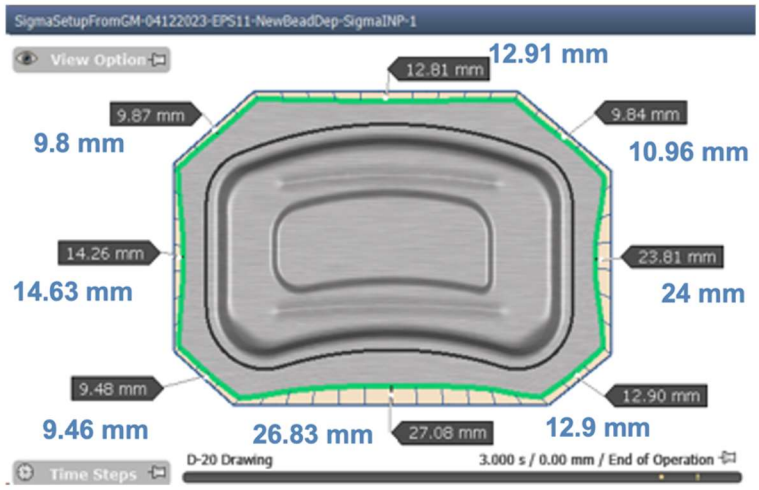

Target Nominal Draw-in Values

Difference: 2.0%

Case 2

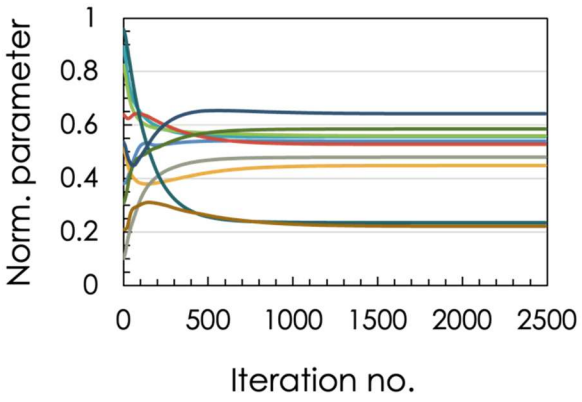

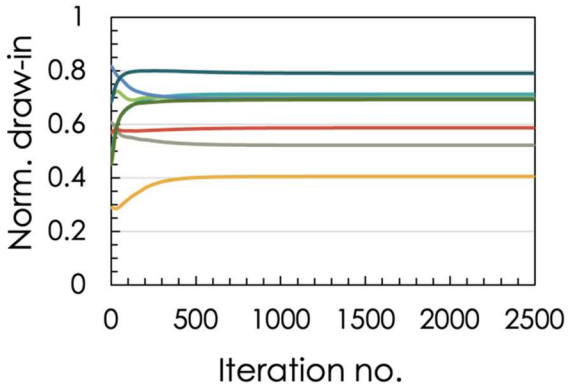

Sim #2

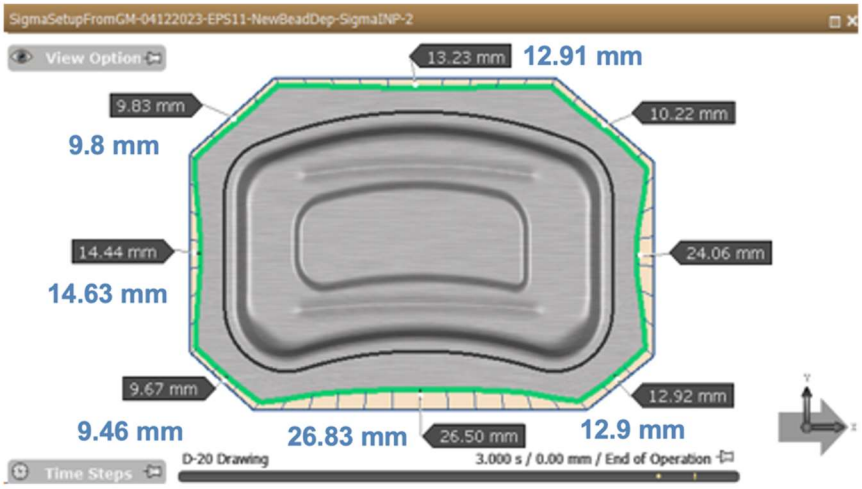

Target Nominal Draw-in Values

Difference: 1.8%

Case 3

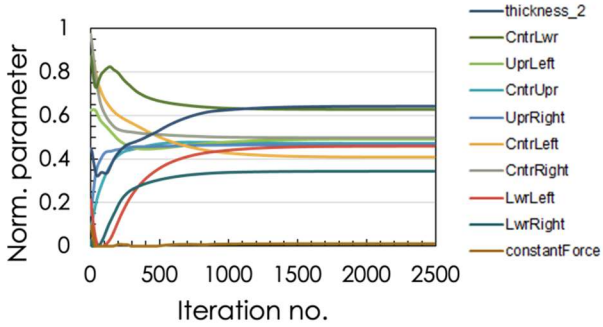

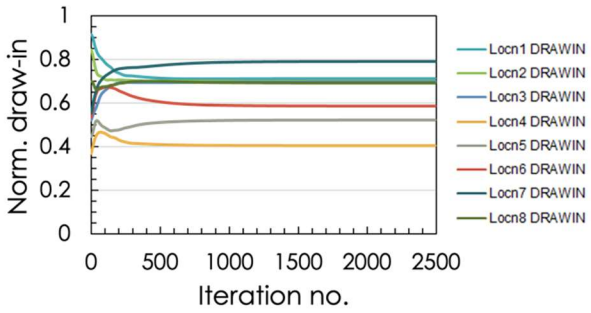

Sim #3

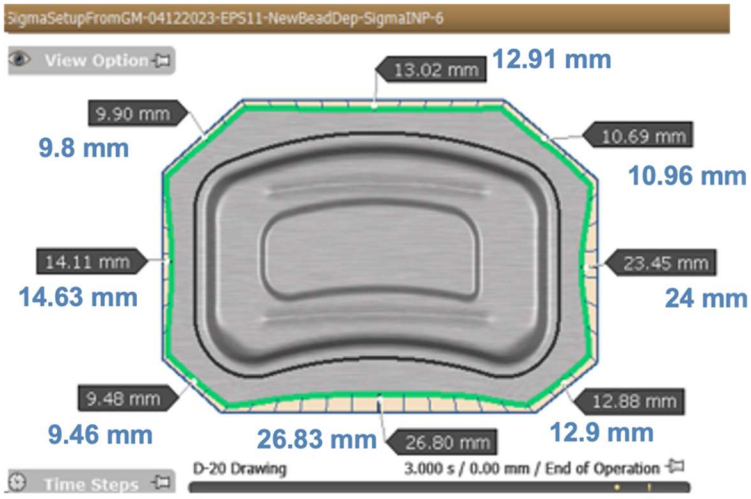

Target Nominal Draw-in Values

Difference: 1.3%

Appendix 4 – Optimization of door panel geometry

#	*Before*	*After*
I	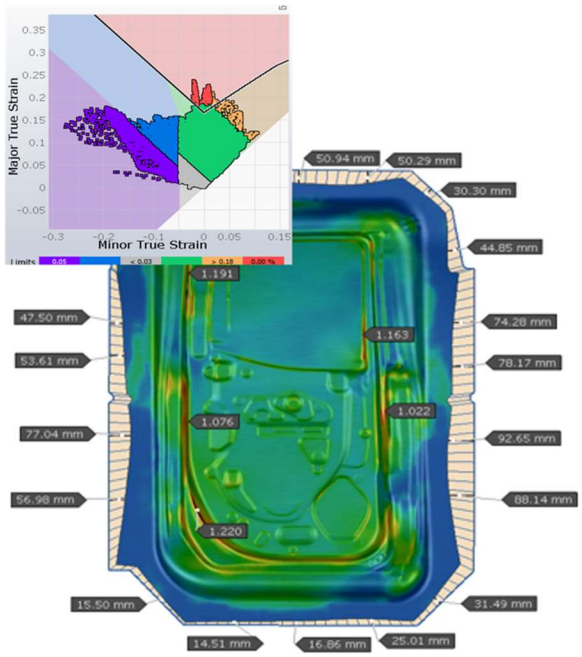	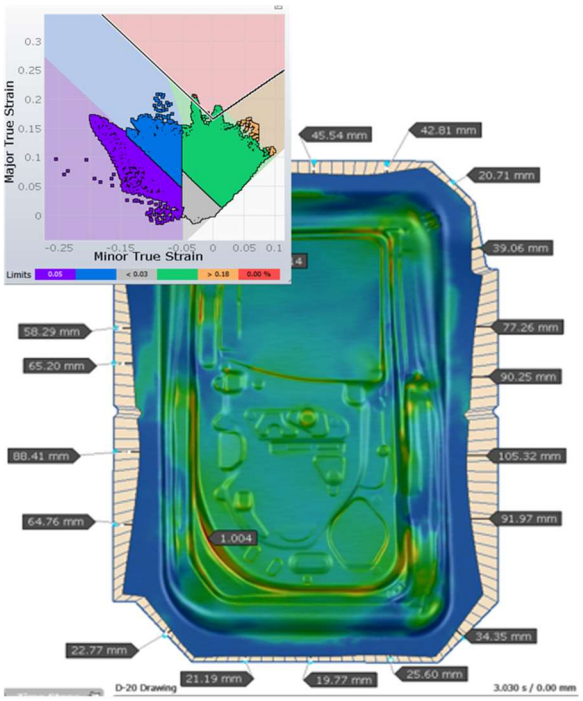
II	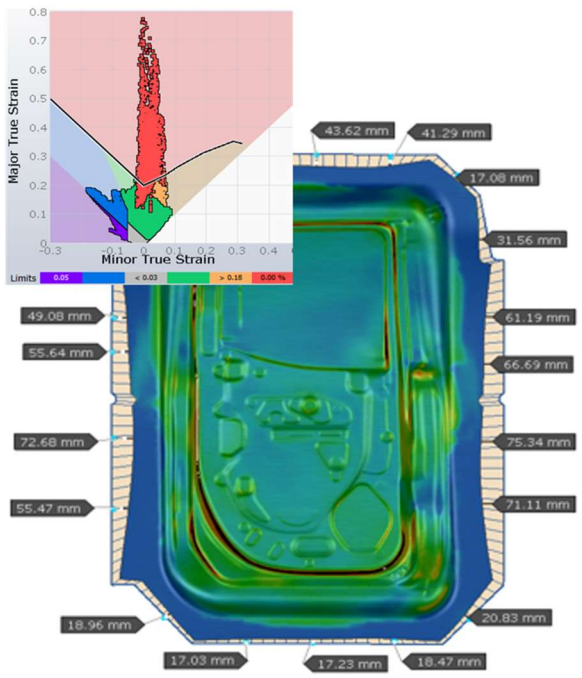	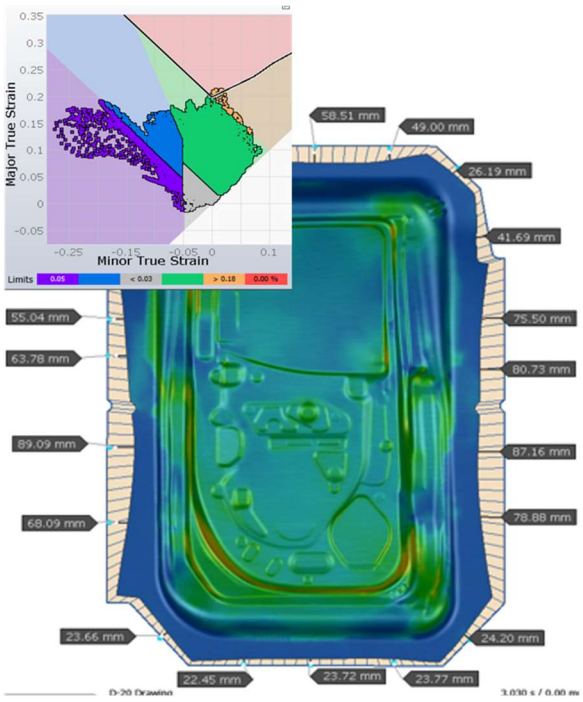

1	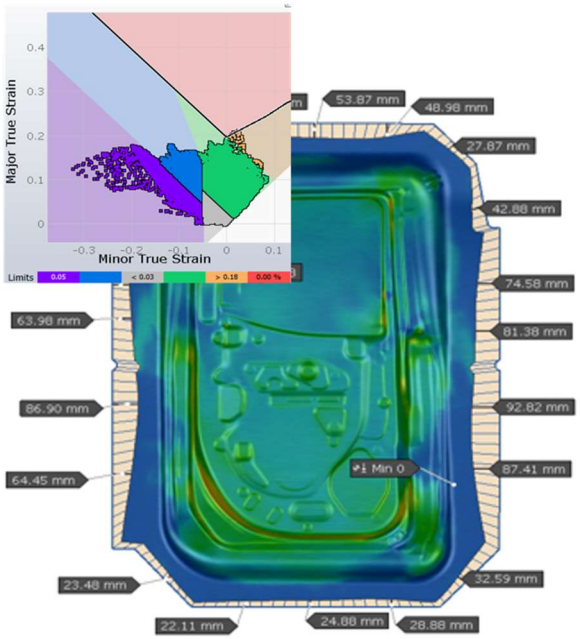 Major True Strain Minor True Strain Limits 53.87 mm 48.98 mm 27.87 mm 42.88 mm 74.58 mm 81.38 mm 92.82 mm 87.41 mm 32.59 mm 28.88 mm 24.88 mm 22.11 mm 23.48 mm 64.45 mm 86.90 mm 63.98 mm Min 0	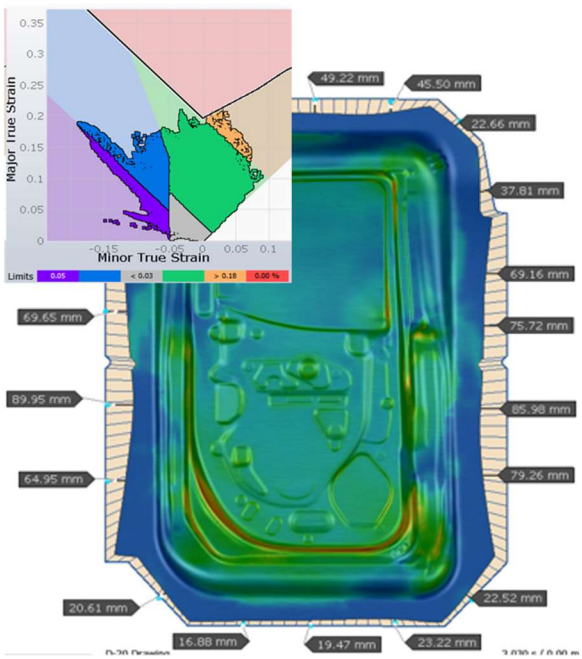 Major True Strain Minor True Strain Limits 49.22 mm 45.50 mm 22.66 mm 37.81 mm 69.16 mm 75.72 mm 85.98 mm 79.26 mm 22.52 mm 23.22 mm 19.47 mm 16.88 mm 20.61 mm 64.95 mm 89.95 mm 69.65 mm
2	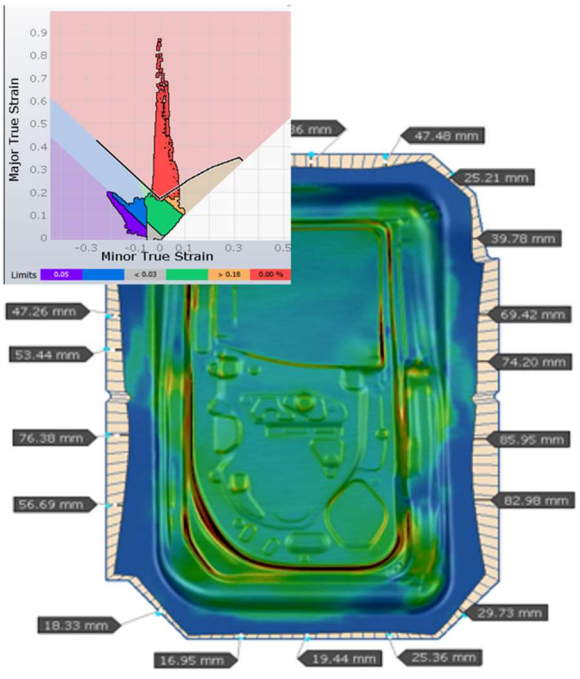 Major True Strain Minor True Strain Limits 47.48 mm 25.21 mm 39.78 mm 69.42 mm 74.20 mm 85.95 mm 82.98 mm 29.73 mm 25.36 mm 19.44 mm 16.95 mm 18.33 mm 56.69 mm 76.38 mm 53.44 mm 47.26 mm	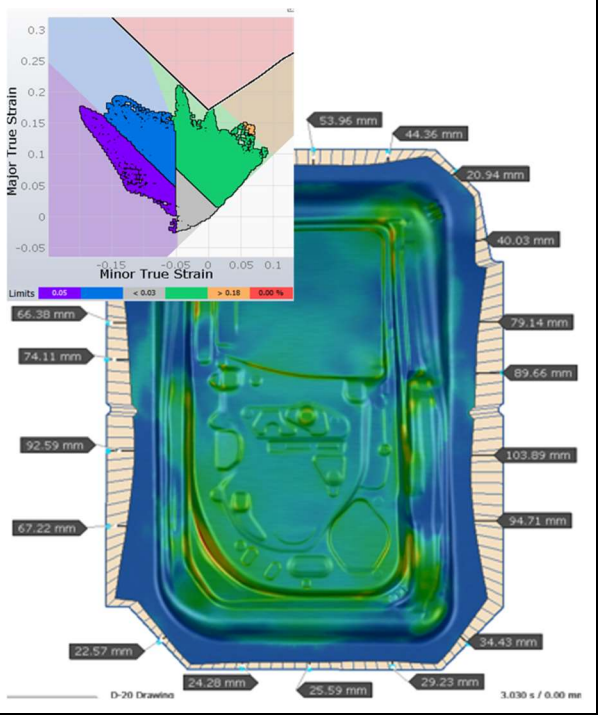 Major True Strain Minor True Strain Limits 53.96 mm 44.36 mm 20.94 mm 40.03 mm 79.14 mm 89.66 mm 103.89 mm 94.71 mm 34.43 mm 29.23 mm 25.59 mm 24.28 mm 22.57 mm 67.22 mm 92.59 mm 74.11 mm 66.38 mm D-20 Drawing 3.030 s / 0.00 mm

3	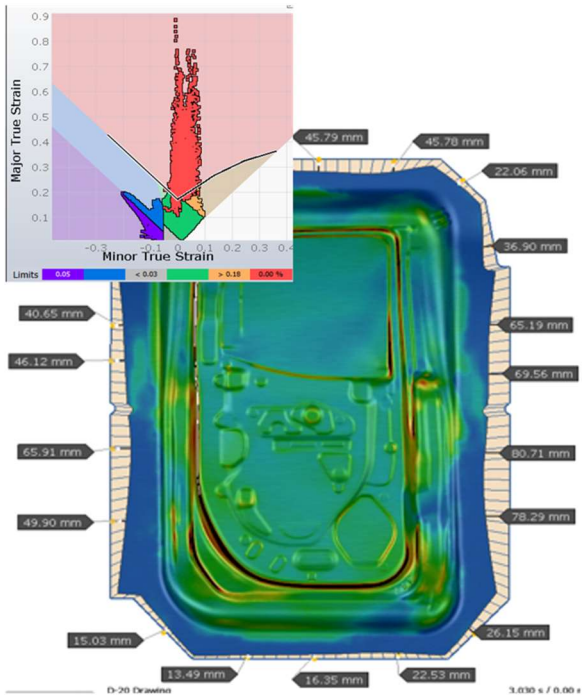 Major True Strain Minor True Strain Limits 45.79 mm 45.78 mm 22.06 mm 36.90 mm 40.65 mm 65.19 mm 46.12 mm 69.56 mm 65.91 mm 80.71 mm 49.90 mm 78.29 mm 15.03 mm 26.15 mm 13.49 mm 16.35 mm 22.53 mm	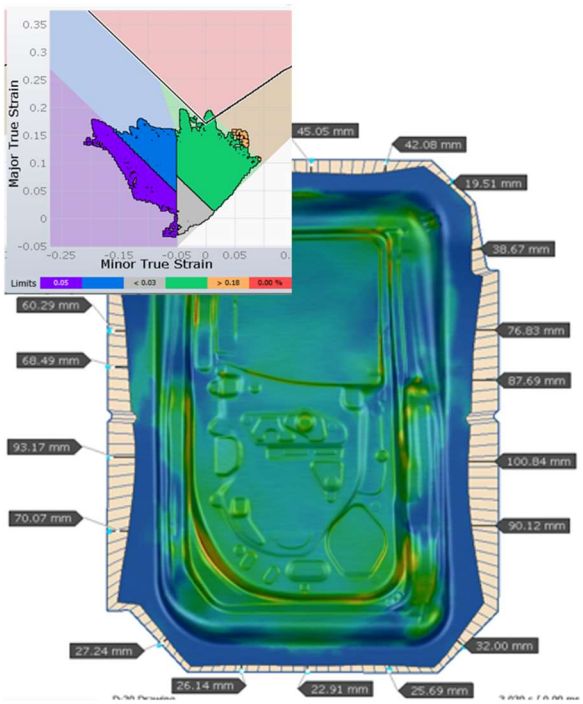 Major True Strain Minor True Strain Limits 45.05 mm 42.08 mm 19.51 mm 38.67 mm 60.29 mm 76.83 mm 68.49 mm 87.69 mm 93.17 mm 100.84 mm 70.07 mm 90.12 mm 27.24 mm 32.00 mm 26.14 mm 22.91 mm 25.69 mm
4	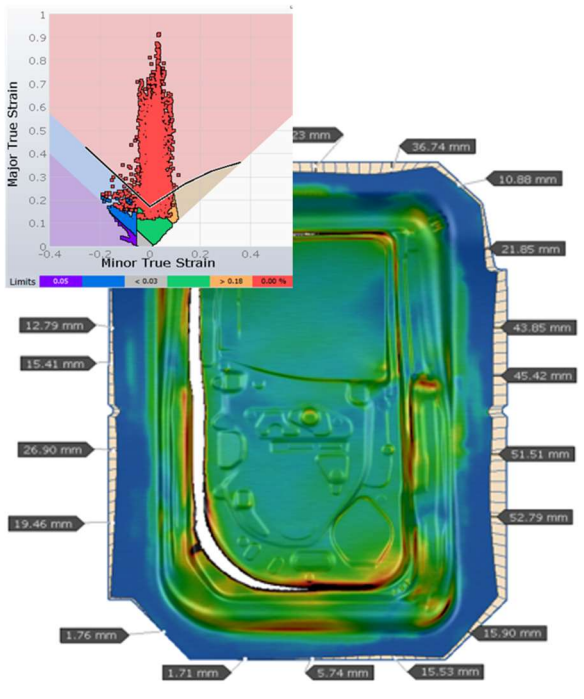 Major True Strain Minor True Strain Limits 36.74 mm 10.88 mm 21.85 mm 12.79 mm 43.85 mm 15.41 mm 45.42 mm 26.90 mm 51.51 mm 19.46 mm 52.79 mm 1.76 mm 15.90 mm 1.71 mm 5.74 mm 15.53 mm	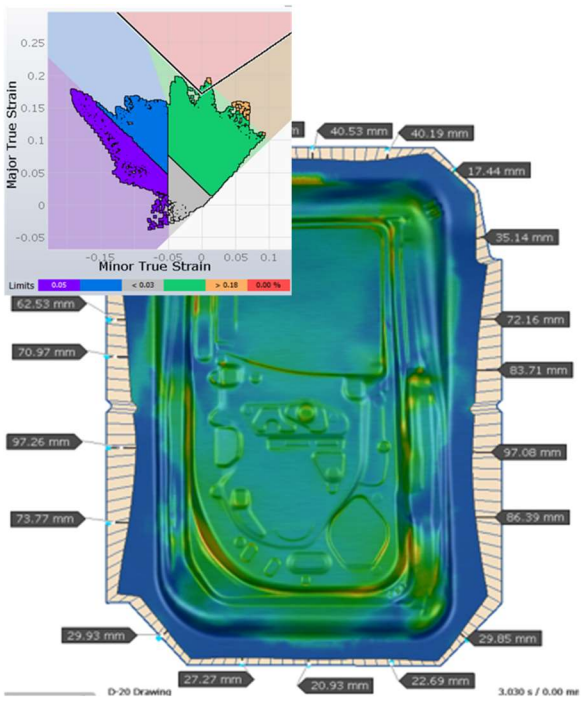 Major True Strain Minor True Strain Limits 40.53 mm 40.19 mm 17.44 mm 35.14 mm 62.53 mm 72.16 mm 70.97 mm 83.71 mm 97.26 mm 97.08 mm 73.77 mm 86.39 mm 29.93 mm 29.85 mm 27.27 mm 20.93 mm 22.69 mm D-20 Drawing 3.030 s / 0.00 ms

5	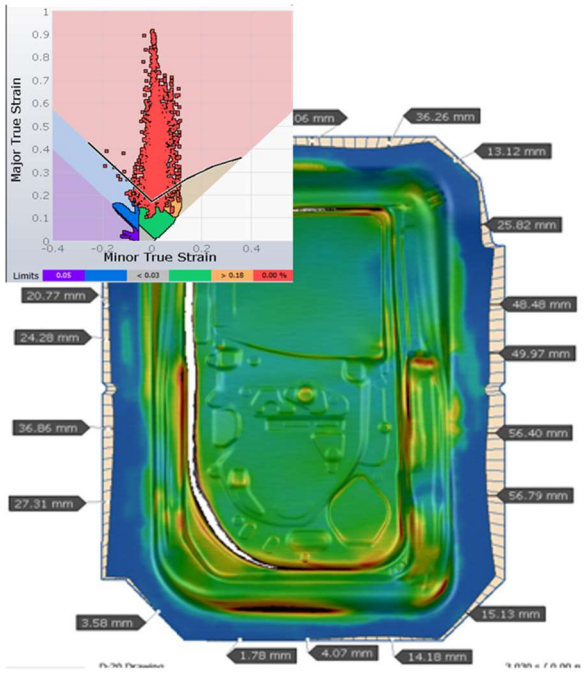 Major True Strain Minor True Strain Limits 0.05 < 0.03 > 0.18 0.00 % 06 mm 36.26 mm 13.12 mm 25.82 mm 48.48 mm 49.97 mm 56.40 mm 56.79 mm 15.13 mm 14.18 mm 4.07 mm 1.78 mm 3.58 mm 27.31 mm 36.86 mm 24.28 mm 20.77 mm	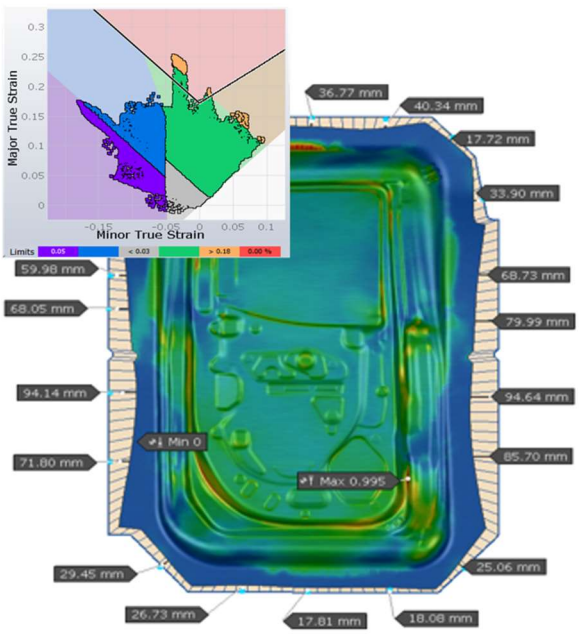 Major True Strain Minor True Strain Limits 0.05 < 0.03 > 0.18 0.00 % 36.77 mm 40.34 mm 17.72 mm 33.90 mm 68.73 mm 79.99 mm 94.64 mm 85.70 mm 25.06 mm 18.08 mm 17.81 mm 26.73 mm 29.45 mm 71.80 mm 94.14 mm 68.05 mm 59.98 mm Min 0 Max 0.995
6	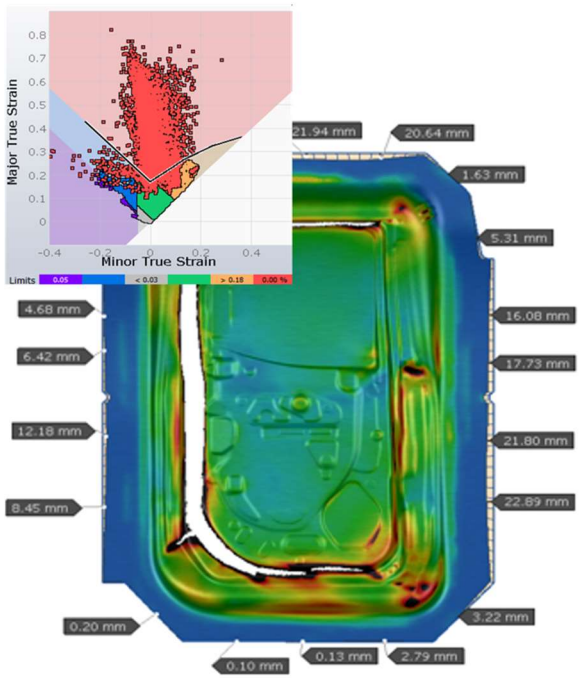 Major True Strain Minor True Strain Limits 0.05 < 0.03 > 0.18 0.00 % 21.94 mm 20.64 mm 1.63 mm 5.31 mm 16.08 mm 17.73 mm 21.80 mm 22.89 mm 3.22 mm 2.79 mm 0.13 mm 0.10 mm 0.20 mm 8.45 mm 12.18 mm 6.42 mm 4.68 mm	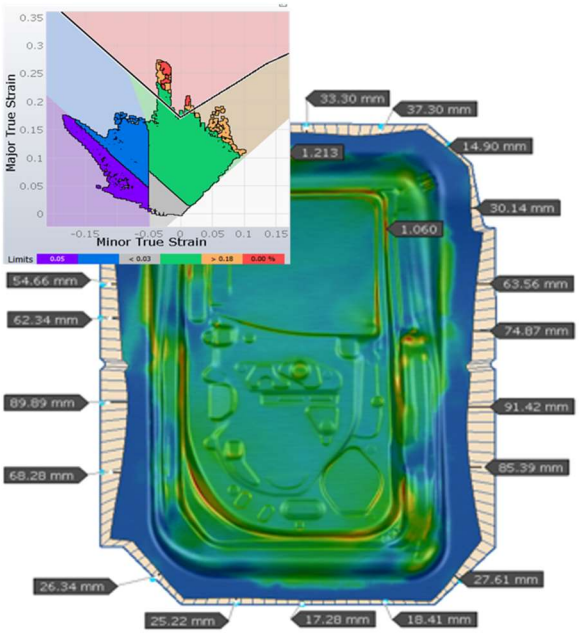 Major True Strain Minor True Strain Limits 0.05 < 0.03 > 0.18 0.00 % 33.30 mm 37.30 mm 14.90 mm 1.213 30.14 mm 1.060 63.56 mm 74.87 mm 91.42 mm 85.39 mm 27.61 mm 18.41 mm 17.28 mm 25.22 mm 26.34 mm 68.28 mm 89.89 mm 62.34 mm 54.66 mm